Weierstraß–Institut

für Angewandte Analysis und Stochastik

im Forschungsverbund Berlin e.V.

Preprint ISSN 0946 – 8633

Thermodynamics–Based Modeling of Edge–Emitting Quantum Well Lasers

U. Bandelow, H. Gajewski, R. Hünlich

submitted: October 7th 2004

Weierstrass Institute for
Applied Analysis and Stochastics
Mohrenstraße 39
D – 10117 Berlin, Germany
E-Mail:
bandelow@wias-berlin.de
gajewski@wias-berlin.de
huenlich@wias-berlin.de

No. 971

Berlin 2004

2000 *Mathematics Subject Classification.* 78A60, 35Q60, 80A20, 35G25, 76M10.
Key words and phrases. Semiconductor lasers, continuity equations, Poisson equation, wave guide equations, photon rate equations, heat flow equation, entropy balance equation, discretization, iteration scheme.

Edited by
Weierstraß–Institut für Angewandte Analysis und Stochastik (WIAS)
Mohrenstraße 39
D — 10117 Berlin
Germany

Fax: + 49 30 2044975
E-Mail: preprint@wias-berlin.de
World Wide Web: http://www.wias-berlin.de/

Summary. This paper describes the modeling and the simulation of edge-emitting quantum well (QW) lasers, based on the drift-diffusion equations and equations for the optical field. By applying fundamental thermodynamic principles as the maximum entropy principle and the principle of local thermal equilibrium we derive a self-consistent energy transport model which can be proven to meet the thermodynamic requirements. It's numerical solution is discussed explicitly, by starting from the discretization procedure and by ending up with the iteration scheme. As an example, we demonstrate the simulation of a long-wavelength ridge-waveguide multi-quantum well laser.

1 Introduction

In modern semiconductor devices such as high power transistors or lasers thermal effects caused by strong electric and optical fields and by strong recombination play an important role and have to be included in the mathematical models.

Indeed, there is a large variety of energy models for semiconductor devices. Typically, these models base on the usual state equations and continuity equations for the carrier densities and on the balance of the total energy expressed by the equation

$$\partial_t u + \nabla \cdot j_u = -\gamma \tag{1}$$

for the density u and the current density j_u of this total energy, where γ counts for the radiation which is emitted from the device. Furthermore, differential relations for u and general thermodynamic relations for j_u are used to transform the energy balance equation (1) into a heat flow equation [1]

$$c_h \partial_t T - \nabla \cdot (\kappa_L \nabla T) = H, \tag{2}$$

where c_h is the heat capacity and κ_L the heat conductivity. While the heat flow equation (2) with the description of the source term H is well established, the discussion about its relation to the conservation law of energy is still ongoing.

In this contribution, based on an expression for the density of the free energy, we derive a thermodynamics-based system of evolution equations for edge-emitting quantum well lasers in a deductive way. Thereby we only apply first principles like the entropy maximum principle and the principle of partial local equilibrium [2]. Moreover, we assume that the free energy is the sum of the internal free energy, of the electrostatic field energy and of the energy of the optical field. For the simulation of semiconductor lasers the energy transport model is coupled to the evolution equations for the optical field in a self-consistent manner. The resulting energy transport model is in this explicit form new to our knowledge and can be shown to meet the thermodynamic requirements. Boundary conditions as well as proper discretization schemes will be discussed too. Furthermore, the numerical solution procedure will be discussed. The complete energy transport model has been implemented in WIAS-TeSCA [3], a numerical code for simulation of semiconductor devices. On this base, we demonstrate the simulation of long-wavelength edge-emitting QW lasers, with a special focus on the self-heating of the device and the modulation response.

2 Basic Equations

Let $\Omega \subset \mathbb{R}^2$ be the transverse cross section of the (possibly hetero-) device under consideration. By ∇ we denote the transverse part of the Nabla operator, i. e., the Nabla operator with respect to $\mathbf{r} = (x, y) \in \Omega$.
We denote by n and p the densities of the mobile charge carriers, electrons and holes, respectively, and by C the net doping profile. For shorter notation these densities as well as the band-edge densities of states N_c and N_v are scaled by a reference density N_{ref}. The lattice temperature T is scaled by a reference temperature T_s. Moreover, the electrostatic potential φ as well as the quasi-Fermi potentials f_n and f_p are scaled by $u_{T_s} = k_B T_s/q$ and the conduction and valence band edges e_c and e_v by $k_B T_s$. Here k_B and q are Boltzmann's constant and the elementary charge, respectively.

2.1 Poisson Equation

The electrostatic potential φ satisfies Poisson's equation

$$-\nabla \cdot (\varepsilon \nabla \varphi) = C + p - n \tag{3}$$

in the transverse cross section Ω of the laser. Here $\varepsilon = \varepsilon(\mathbf{r})$ is the static dielectric constant in the possibly heterogeneous semiconductor material.

2.2 Transport Equations

The charge carrier densities n and p have to fulfill the continuity equations

$$\frac{\partial n}{\partial t} - \nabla \cdot \mathbf{j}_n = -R\,, \tag{4}$$

$$\frac{\partial p}{\partial t} + \nabla \cdot \mathbf{j}_p = -R \tag{5}$$

for $(t, \mathbf{r}) \in \mathbb{R}^1_+ \times \Omega$, i.e. for all times $t > 0$ in the transverse cross section. $\mathbf{j}_n$ denotes the electron current density and $\mathbf{j}_p$ the hole current density. The recombination rate R in (4), (5) involves all non-radiative and radiative recombination processes, as in particular the Shockley-Read-Hall recombination rate R^{SRH}, the Auger recombination rate R^{AUG} and the spontaneous radiative recombination rate R^{sp}. The recombination processes stimulated by the optical field are included by the stimulated recombination rate R^{stim}

$$R^{stim} = v_g g |\chi|^2 N_s \tag{6}$$

where v_g denotes the group velocity and g the material gain. The modal intensity distribution $|\chi|^2$ and the photon number N_s will be discussed in subsection 2.4.

As a consequence of the Poisson equation (3) and the continuity equations (4), (5) we infer the current conservation equation

$$\nabla \cdot \mathbf{j} = 0\,, \quad \mathbf{j} = -\varepsilon \nabla \frac{\partial \varphi}{\partial t} + \mathbf{j}_n + \mathbf{j}_p \tag{7}$$

to hold in $\mathbb{R}^1_+ \times \Omega$.

2.3 State Equations

The quasi-Fermi potentials are linked with the carrier concentrations by means of Fermi-Dirac statistics:

$$n = N_c \mathcal{F}_{1/2}\left(\frac{\varphi - f_n - e_c}{T}\right), \tag{8}$$

$$p = N_v \mathcal{F}_{1/2}\left(\frac{e_v + f_p - \varphi}{T}\right). \tag{9}$$

The size quantization by the quantum wells essentially induces a modified density of states. We simulate this by multi-band kp-models to obtain at least net coefficients which model the QW's like classical materials with specific material parameters. This has been extensively described recently in [4].

2.4 Optics

Assuming stable transverse waveguiding allows us to express the main component of the optical field vector $E(\mathbf{r}, z, t)$

$$E(\mathbf{r}, z, t) = e^{i\omega t}\left[\Psi^+(z,t)e^{-ikz} + \Psi^-(z,t)e^{ikz}\right]\chi(\mathbf{r}) \tag{10}$$

in terms of the transverse main mode χ. Transverse modes χ are eigensolutions of the waveguide equation

$$\left[\nabla^2 + \frac{\omega^2}{c^2}\varepsilon_{opt}(\omega, \mathbf{r}) - \beta^2\right]\chi(\mathbf{r}) = 0, \tag{11}$$

corresponding to their respective (complex) eigenvalues β.[1] Here

$$\varepsilon_{opt}(\omega, \mathbf{r}) = \left(n_r(\omega, \mathbf{r}) + ic\left[g(\omega, \mathbf{r}) - \alpha_{bg}(\mathbf{r})\right]/2\omega\right)^2$$

denotes the complex dielectric function of the pumped laser averaged over one section in longitudinal direction. Via the gain $g(\omega, \mathbf{r})$, the background absorption $\alpha_{bg}(\mathbf{r})$ and the refractive index $n_r(\omega, \mathbf{r})$ the dielectric function ε_{opt} depends on almost all properties of the device and its operating state, as well as on properties of the optical field, as its polarization and its frequency. In consequence the eigenvalues β as well as the eigenfunctions χ will parametrically depend on the carrier density distribution and on the temperature profile as well, both of which can change in time. By modeling this we allow for the corresponding changes of the eigenvalues and of the optical field profile, but we do not allow for explicit time derivatives of β and χ throughout this paper. This is at least due to the very different time scales of the optical and the electro-thermal processes, the latter of which slave the optical processes.

In 2D-simulations with WIAS-TESCA, longitudinal properties are only considered by assuming a longitudinally homogeneous power distribution,

[1] Eq. (11) is formulated here for TE-polarization. TM polarization can be counted for as well, without restrictions for the considerations here, but with a different version of (11).

which is approximately met in Fabry-Perot lasers or in edge-emitting lasers with properly designed Bragg gratings [5]. In our calculations the fundamental mode has been involved, the number of photons N_s of which is balanced by a corresponding photon rate equation

$$\dot{N}_s = v_g(2\Im m\beta - \alpha_0 - \alpha_m)N_s + r^{sp}. \tag{12}$$

In (12) $\dot{N}_s$ is short notation for the time derivative of N_s, r^{sp} is short for the spontaneous emission into the mode, α_0 are the longitudinal scattering losses and

$$\alpha_m = \frac{1}{2L} \ln \frac{1}{R_0 R_L} \tag{13}$$

are the output losses for a Fabry-Perot laser with facet reflectivities R_0 at $z = 0$ and R_L at $z = L$, e.g.. The energy density loss γ

$$\gamma = \hbar\omega v_g(\alpha_0 + \alpha_m)|\chi|^2 N_s. \tag{14}$$

counts the radiation energy which is emitted from the device per time, either by the lasing mode trough the end facets (α_m) or by the excitation of other modes (α_0).

The modal gain $2\Im m\beta$ is the imaginary part of the corresponding eigenvalue subject to (11). For the modal gain $2\Im m(\beta)$ an alternative expression can be obtained from (11) in first order of perturbation theory:

$$2\Im m(\beta) = \int (g - \alpha_{bg})|\chi|^2 d\Omega. \tag{15}$$

The photon rate equation (12) is valid for Fabry-Perot and Bragg resonators with a homogeneous longitudinal field distribution. The intensity distribution of the lasing mode along the transverse plane is readily obtained by multiplying N_s with the (suitable normalized) transverse intensity distribution $|\chi|^2$ of the lasing mode. The photon flow over the boundary of the transverse domain Ω is neglectible as long as the lasing mode is a guided mode, what we will assume throughout this paper.

3 Heating

Recently, the drift-diffusion model (3)-(5) has been coupled to a heat transport equation [2]. In this section we want to motivate the heat transport equation and the resulting energy model by considering fundamental thermodynamic requirements. For the sake of simplicity we restrict us here to the case of Boltzmann statistics.

3.1 Free Energy, Entropy, Energy

We define densities of free energy f, entropy s and energy u by

$$f = \frac{\varepsilon}{2}|\nabla\varphi|^2 + c_L T(1-\log T) + u_{rad} - Ts_{rad}$$
$$+n[T(\log\frac{n}{N_c} - 1) + e_c] + p[T(\log\frac{p}{N_v} - 1) - e_v] \,, \tag{16}$$
$$s = -\frac{\partial f}{\partial T} = nP_n + pP_p + c_L \log T + s_{rad}, \tag{17}$$
$$u = f + Ts = \frac{\varepsilon}{2}|\nabla\varphi|^2 + c_L\, T + u_n n + u_p p + u_{rad}. \tag{18}$$

Here c_L is the lattice heat capacity, the prime $'$ means differentiation with respect to temperature T and

$$P_n = 1 + R_n - \log\left(\frac{n}{N_c}\right) - e_c', \quad R_n = T(\log N_c)', \tag{19}$$
$$P_p = 1 + R_p - \log\left(\frac{p}{N_v}\right) + e_v', \quad R_p = T(\log N_v)', \tag{20}$$

are the entropies per electron and hole, respectively. The energies per particle u_n and u_p are defined by

$$u_n = T(R_n - 1) + e_c - Te_c' \tag{21}$$
$$u_p = T(R_p - 1) - e_v + Te_v' \tag{22}$$

for electrons and holes, respectively. For completeness we note ($e_g = e_c - e_v$):

$$u_n + u_p = T(R_n + R_p) + e_g - Te_g' = T(P_n - 1) + T(P_p - 1) + (f_p - f_n). \tag{23}$$

Throughout this paper we assume R_n and R_p to be independent on T. The energy density u_{rad} and the entropy density s_{rad} of the optical field are given by (c.f. [6])

$$u_{rad} = \int \rho_{rad}\hbar\omega|\chi|^2 N_s d\hbar\omega \,, \tag{24}$$
$$s_{rad} = k\int \rho_{rad}|\chi|^2\left[(N_s+1)\log(N_s+1) - N_s\log(N_s)\right] d\hbar\omega, \tag{25}$$

where $\rho_{rad} = \frac{8\pi n_r^3(\hbar\omega)^2}{h^3c^3}$ is the density of states for the photons [7].

Then, we define free energy F, entropy S and energy U by

$$F = \int_\Omega f\, d\Omega \,, \quad S = \int_\Omega s\, d\Omega \,, \quad U = \int_\Omega u\, d\Omega \,. \tag{26}$$

To find equilibrium values for n, p and T we maximize the entropy S under the constraints

$$Q = \int_\Omega (C + p - n)\, d\Omega = const., \quad U = const. \,. \tag{27}$$

Following Lagrange's method, this can be done by maximizing the augmented entropy

$$S_\lambda = S + \lambda\, Q \; + \lambda_3 U \; . \tag{28}$$

The resulting Euler-Lagrange-equations read

$$\lambda_3 = -\frac{1}{T}\;, \quad q_{n,p}\lambda = \partial_{n,p}\Big[S - \frac{U}{T}\Big], \quad q_p = 1 = -q_n, \quad \log\left(\frac{N_s+1}{N_s}\right) = \frac{\hbar\omega}{T}\;,$$

with constant Lagrange multipliers λ and λ_3. Solving these equations for n, p and N_s, we arrive at the Bose distribution for the photons [2]

$$n_s = \frac{1}{1-\exp\left(\frac{\hbar\omega}{T}\right)}. \tag{29}$$

and the state equations (8) and (9) but according to Boltzmann statistics:

$$n = N_c \exp\left(\frac{\varphi - f_n - e_c}{T}\right), \quad p = N_v \exp\left(\frac{e_v + f_p - \varphi}{T}\right) \tag{30}$$

and with coinciding constant equilibrium quasi-Fermi potentials defined by (c.f. (8), (9))

$$\frac{f_n}{T} = \frac{f_p}{T} = \lambda. \tag{31}$$

3.2 Current Densities

According to the principle of local thermal equilibrium we assume the state equations (8), (9) respectively (30), to be hold also in the case of different, non constant quasi-Fermi potentials f_n, f_p and non-homogeneous temperature T. Moreover, we suppose the vector $\nabla\boldsymbol{\lambda} = (\nabla\lambda_1, \nabla\lambda_2, \nabla\lambda_3)$ of gradients of Lagrange multipliers

$$\lambda_1 = \frac{f_n}{T}, \quad \lambda_2 = \frac{f_p}{T}, \quad \lambda_3 = -\frac{1}{T} \tag{32}$$

to be driving force towards to equilibrium, i. e., we make the ansatz

$$\mathbf{j} = (0, 0, \varphi\dot{\mathbf{D}}) - L\,\nabla\boldsymbol{\lambda}, \quad \mathbf{j} = (\mathbf{j}_n, \mathbf{j}_p, \mathbf{j}_u)\;, \tag{33}$$

with a (3×3) conductivity-matrix L, which has to be positively definite and symmetric in view of the second law of thermodynamics and Onsager's reciprocity relations. $\dot{\mathbf{D}} = -\varepsilon\nabla\varphi_t$ is the electric displacement current density. [3] We specify L such that (33) becomes

[2] In [8] a generalization of (29) can be found. There, n_s is the average optical-mode occupation factor of photons which are in (a hypothetical) equilibrium with a biased semiconductor, where the carriers separated by $f_p - f_n$. Such a hypothetical equilibrium can only occur if the photons are associated with an optical cavity that is closed and loss-free, except for optical transitions between conduction and valence band [8].

[3] Note that due to perfect optical waveguiding the optical energy flow is only along the z-axis and hence doesn't occur in the flow (33) along the transverse plane.

$$\mathbf{j}_n = T\Big[-(\sigma_n+\sigma_{np})\nabla\lambda_1+\sigma_{np}\nabla\lambda_2+[\sigma_n(P_n-\lambda_1)-\sigma_{np}(\lambda_1-\lambda_2)]\nabla\lambda_3\Big]\,,$$
$$\mathbf{j}_p = T\Big[-(\sigma_p+\sigma_{np})\nabla\lambda_2+\sigma_{np}\nabla\lambda_1-[\sigma_p(P_p+\lambda_2)+\sigma_{np}(\lambda_1-\lambda_2)]\nabla\lambda_3\Big]\,,$$
$$\begin{aligned}\mathbf{j}_u = &-\varphi\varepsilon\nabla\varphi_t - T^2[\kappa_L\nabla T+(P_n-\lambda_1)^2+(P_p+\lambda_2)^2+\sigma_{np}(\lambda_1-\lambda_2)^2]\nabla\lambda_3\\ &+T[\sigma_n(P_n-\lambda_1)-\sigma_{np}(\lambda_1-\lambda_2)]\nabla\lambda_1\\ &-T[\sigma_p(P_p+\lambda_2)-\sigma_{np}(\lambda_2-\lambda_1)]\nabla\lambda_2\,,\end{aligned}\tag{34}$$

where

$$\sigma_n = a\,n\mu_n,\quad \sigma_p = a\,p\mu_p\,,\quad \sigma_{np}=\sigma_{pn}=a\,np\mu_n\mu_p\,b\,,\tag{35}$$
$$b=\frac{c_1[1+c_2(n+p)/2]}{1+c_3(n+p)/2}\,,\quad a=\frac{1}{1+(p\mu_n+n\mu_p)b}\,,\tag{36}$$

and $\mu_n, \mu_p, c_1, c_2, c_3$ and κ_L are material parameters (see [9, 10]). It is worth to note, that the appearance of $\varphi\varepsilon\nabla\varphi_t$ in $\mathbf{j}_u$ is a feature of our model. Replacing $\nabla\boldsymbol{\lambda}$ by the more familiar vector $(\nabla f_n, \nabla f_p, \nabla T)$, we can rewrite the current densities as

$$\mathbf{j}_n = -\sigma_n(\nabla f_n - P_n\nabla T)+\sigma_{np}[\nabla(f_p-f_n)+(P_n+P_p)\nabla T]\,,\tag{37}$$
$$\mathbf{j}_p = -\sigma_p(\nabla f_p + P_p\nabla T)+\sigma_{pn}[\nabla(f_n-f_p)-(P_n+P_p)\nabla T]\,,\tag{38}$$
$$\mathbf{j}_u = -\varphi\varepsilon\nabla\varphi_t-\kappa_L\nabla T-(P_nT-f_n)\mathbf{j}_n+(P_pT+f_p)\mathbf{j}_p\,.\tag{39}$$

For later use we define here also the temperature current density $\mathbf{j}_T$ and the heat current density $\mathbf{j}_q$ by

$$\mathbf{j}_T = -\kappa_L\nabla T - T(P_n\mathbf{j}_n - P_p\mathbf{j}_p)\tag{40}$$
$$\mathbf{j}_q = -\kappa_L\nabla T.\tag{41}$$

3.3 Heat Equation

Now we can transform the energy balance equation (1) into a heat flow equation. With the heat capacity

$$c_h = c_L + nu_n' + pu_p'\,,\tag{42}$$

we find by using the current conservation equation (7) and the definition of the energy u,

$$\begin{aligned}\frac{\partial u}{\partial t} &= \varepsilon\nabla\varphi\cdot\nabla\varphi_t + c_hT_t + n_tu_n + p_tu_p + \partial_t u_{rad}\\ &= \varepsilon\nabla\varphi\cdot\nabla\varphi_t+\varphi(\nabla\cdot(\varepsilon\nabla\varphi_t)+p_t-n_t)+c_hT_t+n_tu_n+p_tu_p+\partial_tu_{rad}\\ &= \nabla\cdot(\varphi\varepsilon\nabla\varphi_t)+c_hT_t+n_t(u_n-\varphi)+p_t(u_p+\varphi)+\partial_tu_{rad}\,.\end{aligned}\tag{43}$$

We note

$$u_n-\varphi = T(P_n-1)-f_n\tag{44}$$
$$u_p+\varphi = T(P_p-1)+f_p.\tag{45}$$

We insert now (43) and (39) in the energy balance equation (1):

$$c_h T_t + n_t(u_n - \varphi) + p_t(u_p + \varphi) + \partial_t u_{rad} + \nabla \cdot \mathbf{j}_T + \nabla \cdot (f_n \mathbf{j}_n + f_p \mathbf{j}_p) = -\gamma. \quad (46)$$

Hence

$$\begin{aligned} c_h T_t + \nabla \cdot \mathbf{j}_T &= -n_t(u_n - \varphi) - p_t(u_p + \varphi) - \partial_t u_{rad} - \nabla \cdot (f_n \mathbf{j}_n + f_p \mathbf{j}_p) - \gamma \\ &= -(u_n - \varphi)(\nabla \cdot \mathbf{j}_n + R) + (u_p + \varphi)(\nabla \cdot \mathbf{j}_p + R) \\ &\quad -\partial_t u_{rad} - \nabla \cdot (f_n \mathbf{j}_n + f_p \mathbf{j}_p) - \gamma \\ &= (u_n + u_p)R - \partial_t u_{rad} - \gamma - TP_n \nabla \cdot \mathbf{j}_n + TP_p \nabla \cdot \mathbf{j}_p \\ &\quad +T(\nabla \cdot \mathbf{j}_n - \nabla \cdot \mathbf{j}_p) - \mathbf{j}_n \cdot \nabla f_n - \mathbf{j}_p \cdot \nabla f_p \\ &= (u_n + u_p)R - \partial_t u_{rad} - \gamma - TP_n \nabla \cdot \mathbf{j}_n + TP_p \nabla \cdot \mathbf{j}_p \\ &\quad +T\nabla \cdot (\mathbf{j}_n - \mathbf{j}_p) - \mathbf{j}_n \cdot (\nabla f_n - P_n \nabla T) \\ &\quad -\mathbf{j}_p \cdot (\nabla f_p + P_p \nabla T) - P_n \nabla T \cdot \mathbf{j}_n - P_p \nabla T \cdot \mathbf{j}_p \end{aligned}$$

Replacing now $\mathbf{j}_T$ by $\mathbf{j}_q$ (41) we find

$$\begin{aligned} c_h T_t + \nabla \cdot \mathbf{j}_q = \nabla \cdot T(P_n \mathbf{j}_n - P_p \mathbf{j}_p) &- TP_n \nabla \cdot \mathbf{j}_n - P_n \nabla T \cdot \mathbf{j}_n \\ &+TP_p \nabla \cdot \mathbf{j}_p + P_p \nabla T \cdot \mathbf{j}_p + T\nabla \cdot (\mathbf{j}_n - \mathbf{j}_p) \\ &+(u_n + u_p)R - \partial_t u_{rad} - \gamma \\ &-\mathbf{j}_n \cdot (\nabla f_n - P_n \nabla T) - \mathbf{j}_p \cdot (\nabla f_p + P_p \nabla T) \end{aligned}$$

and by straightforward calculation finally the desired heat flow equation (2)

$$c_h T_t - \nabla \cdot \kappa_L \nabla T = H \quad (47)$$

with the heat source term H

$$\begin{aligned} H = T\nabla P_n \cdot \mathbf{j}_n - T\nabla P_p \cdot \mathbf{j}_p + T\nabla \cdot (\mathbf{j}_n - \mathbf{j}_p) \\ -\mathbf{j}_n \cdot (\nabla f_n - P_n \nabla T) - \mathbf{j}_p \cdot (\nabla f_p + P_p \nabla T) \\ +(u_n + u_p)R - \partial_t u_{rad} - \gamma. \end{aligned} \quad (48)$$

The first two terms on the right hand side of (48) represent the Thomson-Peltier heat, which can be positive and negative as well. The term in the 2nd row of (48) is the Joule heating which is stictly positive. The 1st term in the last row of (48) is the recombination heat. Each recombining electron-hole pair sets free its energy $u_n + u_p$ which is immediately transferred to the lattice, unless it is transferred to the radiation field. This latter radiative part does not heat the device and has therefore to be subtracted from the heat source, as indicated by the appearance of $-\partial_t u_{rad}$ in (48). Similarly, γ counts the total energy loss from our system, see Eq. (1), which cools down the device too. So far, in the stationary case ($\partial_t \mathbf{D} = 0$) our model does not differ from [1] and [11]. Concerning the non-stationary case there are differences to [1] and [11], with respect to the electrostatic potential φ and with respect to the definition of u and $\mathbf{j}_u$, which is required by the conservation of energy.

In particular, H contains contributions H_{rad} from radiative processes:

$$H_{rad} = [R^{sp} + R^{stim}]\,(u_n + u_p) - \partial_t u_{rad} - \gamma \tag{49}$$

which have to be modeled in the following. Thereby we will restrict our consideration to the lasing mode, because it gives the main contribution above threshold. For this, we note

$$T\partial_t s_{rad} = \partial_t u_{rad} = \hbar\omega|\chi|^2 \dot{N}_s. \tag{50}$$

For the lasing mode the energy balance (50) is governed by the global equation (12). To get the local heat sources we have to model the localization of $\dot{N}_s$ in the **r**-plane. For this purpose we assume that the carriers generated by absorption of the lasing field transfer their energy to the lattice directly, without traveling. We use (15) and remove the integral $\int d\Omega$ from all terms to find in this approximation

$$\partial_t u_{rad} = \hbar\omega v_g (g - \alpha_{bg})|\chi|^2 N_s - \gamma + \hbar\omega|\chi|^2 r^{sp}, \tag{51}$$

for the energy density averaged along the laser axis. [4] Then, we obtain

$$\begin{aligned} H_{rad} = {} & \hbar\omega|\chi|^2 v_g \alpha_{bg} N_s - v_g g|\chi|^2 N_s\,[\hbar\omega - (u_p + u_n)] \\ & - [\hbar\omega r^{sp} - (u_p + u_n) R^{sp}] \end{aligned} \tag{52}$$

which is the net heat source caused by the lasing mode. The first terms in (52) describes the background absorption of radiation. It is a strictly positive contribution which dominates H_{rad} above the laser threshold. The second term in (52) is caused by a possible incomplete energy transfer from the carrier ensemble to the radiation field during stimulated processes, which heats the device. The last term deals with the spontaneous emission and can only be discussed reasonably together with the complete radiation field, i.e. including the incoherent radiation field too, which we can not calculate at this time. In our simulations we have dropped the two last terms of (52) for simplicity. [5]

3.4 Entropy Balance

We first note the following relations between the entropies of the electron- and hole subsystem $s_n = nP_p$, $s_p = pP_p$ and the specific entropies per particle P_n, P_p:

[4] The change $\partial_t u_{rad}$ of the energy density of the total radiation field might be the sum over the balances (51) for all modes, at least in the case if they are uncorrelated.

[5] This corresponds to the assumption, that all the radiative recombination processes directly create/annihilate photons, without energy loss. However, also the absorption of the incoherent field would heat the device, but it's calculation remains an open problem here.

$$\frac{\partial s_n}{\partial n} = P_n + n\frac{\partial P_n}{\partial n} = P_n - n\frac{1}{n} = P_n - 1 \tag{53}$$

$$\frac{\partial s_p}{\partial p} = P_p + p\frac{\partial P_p}{\partial p} = P_p - p\frac{1}{p} = P_p - 1 \tag{54}$$

$$\begin{aligned}\frac{\partial(s_n + s_p)}{\partial T} &= n\frac{\partial P_n}{\partial T} + p\frac{\partial P_p}{\partial T} = n(\frac{R_n}{T} - e_c'') + p(\frac{R_p}{T} + e_v'') \\ &= \frac{n}{T}\frac{\partial u_n}{\partial T} + \frac{p}{T}\frac{\partial u_p}{\partial T}\end{aligned} \tag{55}$$

Equipped with that we differentiate now the entropy density (17) with respect to time

$$\begin{aligned}\frac{\partial s}{\partial t} &= c_L T_t/T + n_t(P_n - 1) + p_t(P_p - 1) + \left(\frac{n}{T}\frac{\partial u_n}{\partial T} + \frac{p}{T}\frac{\partial u_p}{\partial T}\right) T_t + \partial_t s_{rad} \\ &= n_t(P_n - 1) + p_t(P_p - 1) + c_h T_t/T + \partial_t s_{rad} \\ &= n_t(P_n - 1) + p_t(P_p - 1) + \frac{1}{T}\nabla\cdot\kappa_L\nabla T + H/T + \partial_t s_{rad} \\ &= (P_n - 1)(\nabla\cdot\mathbf{j}_n - R) - (P_p - 1)(\nabla\cdot\mathbf{j}_p + R) + \frac{1}{T}\nabla\cdot\kappa_L\nabla T \\ &\quad +\nabla P_n\cdot\mathbf{j}_n - \nabla P_p\cdot\mathbf{j}_p + \nabla\cdot(\mathbf{j}_n - \mathbf{j}_p) \\ &\quad -\frac{1}{T}\left(\mathbf{j}_n\cdot(\nabla f_n - P_n\nabla T) - \mathbf{j}_p\cdot(\nabla f_p + P_p\nabla T)\right) \\ &\quad +\frac{1}{T}(u_n + u_p)R + \partial_t s_{rad} - \frac{1}{T}\partial_t u_{rad} - \gamma/T \\ &= \nabla\cdot(P_n\mathbf{j}_n - P_p\mathbf{j}_p) + \frac{1}{T}\nabla\cdot\kappa_L\nabla T \\ &\quad -\frac{1}{T}\left(\mathbf{j}_n\cdot(\nabla f_n - P_n\nabla T) - \mathbf{j}_p\cdot(\nabla f_p + P_p\nabla T)\right) \\ &\quad +\left(\frac{u_n + u_p}{T} - P_n + 1 - P_p + 1\right)R + \partial_t s_{rad} - \frac{1}{T}\partial_t u_{rad} - \gamma/T \\ &= \nabla\cdot\left(\frac{\kappa_L}{T}\nabla T + P_n\mathbf{j}_n - P_p\mathbf{j}_p\right) + \frac{1}{T^2}\cdot\kappa_L|\nabla T|^2 \\ &\quad -\frac{1}{T}\left(\mathbf{j}_n\cdot(\nabla f_n - P_n\nabla T) + \mathbf{j}_p\cdot(\nabla f_p + P_p\nabla T)\right) \\ &\quad +(f_p - f_n)R + \partial_t s_{rad} - \frac{1}{T}\partial_t u_{rad} - \gamma/T,\end{aligned} \tag{56}$$

where we have used (23) and the identity

$$\frac{1}{T}\nabla\cdot\kappa_L\nabla T = \nabla\cdot\frac{\kappa_L}{T}\nabla T + \frac{1}{T^2}\cdot\kappa_L|\nabla T|^2. \tag{57}$$

Eq. (56) is a continuity equation for the entropy density s

$$\frac{\partial s}{\partial t} + \nabla\cdot\mathbf{j}_s = d/T, \tag{58}$$

with the entropy current density $\mathbf{j}_s = \mathbf{j}_T/T$ defined by (40) and the dissipation rate d

$$d = \frac{\kappa_L}{T}|\nabla T|^2 + \sigma_n|\nabla f_n - P_n\nabla T|^2 + \sigma_p|\nabla f_p + P_p\nabla T|^2 \\ +\sigma_{np}|\nabla(f_n - f_p) - (P_n + P_p)\nabla T|^2 + (f_p - f_n)R - \gamma. \qquad (59)$$

The dissipation rate d in (59) is always positive for a device which is isolated from the outside world ($\gamma = 0$). Therefore, by partial integration of (58) and supposing no-flux boundary conditions and $\gamma = 0$ it follows, according to the second law of thermodynamics,

$$\frac{dS}{dt} = \int_\Omega \frac{ds}{dt}\, d\Omega = \int_\Omega \frac{d}{T}\, d\Omega \geq 0\,. \qquad (60)$$

In conclusion, as a feature, we are able to proof the thermodynamic correctness of our model in view of the second law of thermodynamics (60).

4 Boundary Conditions

Let $\Gamma = \partial\Omega$ be the boundary of the transverse cross section Ω of the device under consideration and let $\boldsymbol{\nu}$ be the normal unit vector at any point $\mathbf{r}_\Gamma \in \Gamma$. In order to describe non equilibrium situations we have to complete the system (3), (4), (5), (47) and (11) of coupled nonlinear partial differential equations by boundary conditions. To include homogeneous and non-homogeneous as well Dirichlet- as Neumann-conditions, we choose the form

$$\begin{aligned} \boldsymbol{\nu}\cdot(\varepsilon\nabla\varphi) + \alpha_\varphi(\varphi - \varphi_\Gamma) &= 0\,, \\ \boldsymbol{\nu}\cdot\mathbf{j}_n + \alpha_n(n - n_\Gamma) &= 0\,, \\ \boldsymbol{\nu}\cdot\mathbf{j}_p - \alpha_p(p - p_\Gamma) &= 0\,, \\ \boldsymbol{\nu}\cdot\mathbf{j}_q + \alpha_T(T - T_\Gamma) &= 0\,, \\ \boldsymbol{\nu}\cdot\nabla\chi + \alpha_\chi(\chi - \chi_\Gamma) &= 0\,, \end{aligned} \qquad (61)$$

where $\alpha_\varphi, \alpha_n, \alpha_p, \alpha_T, \alpha_\chi \in (\Gamma \to \mathbb{R}^1)$ and $\varphi_\Gamma, n_\Gamma, p_\Gamma, T_\Gamma, \chi_\Gamma \in (\Gamma \to \mathbb{R}^1)$ are given coefficients and boundary values, respectively. By choosing α very small one can manage homogeneous Neumann-conditions, which means that there will be no flux over the boundary of the domain. This applies e.g. for the temperature at the surface-to-the-air contacts of a device. On the other hand, by choosing α very large one can manage Dirichlet-conditions, which fix the quantity to the value given at the boundary. The latter applies e.g. for the temperature at the heat-sink contact of the device. Finite values of α model at least finite penetration depth's of the quantity into the outside world.
In some situations, for instance to describe the interaction of the device with outer circuits, it is appropriate to replace the boundary condition for the Poisson equation by a (possibly nonlocal) boundary condition for the current conservation equation (7).

5 Discretization

5.1 Time Discretization

In order to maintain a Clausius-Duhem relation like (60) and to get numerically stable algorithms, we use an Euler-backwards time discretization scheme. Accordingly, we replace the time derivatives in the equations (4), (5), (47) by backward difference quotients, that means

$$w_\tau(t,\mathbf{r}) = \frac{1}{\tau}(w(t,\mathbf{r}) - w(t-\tau,\mathbf{r}))\ , \tag{62}$$

where t is the time, $\tau > 0$ is the (backward) time step and $\mathbf{r} = (x,y) \in \Omega$ is a space point. The remaining terms in these equations as well as in the equations (3) and (11) are taken at the time level t.

5.2 Space discretization

For the spatial discretization of the system (3), (4), (5), (47), (11) completed by the boundary conditions (61) we apply the finite volume method. Accordingly to that method we suppose to have triangulation $\{E_l,\ l = 1,...,n_e\}$, such that

$$\Omega = \cup_{l=1}^{n_e} E_l\ .$$

Let n_v be the number of vertices of that triangulation, i. e., the number of elements of the set $\{v_i\ : E_l = (v_i, v_j, v_k),\ 1 \le l \le n_e\}$. We assign to each vertex $v_i = (x_i, y_i)$ its Voronoi volume V_i and its Voronoi surface ∂V_i defined by

$$V_i = \{\mathbf{r} \in \mathbb{R}^2\ : |\mathbf{r} - v_i| < |\mathbf{r} - v_j|\ , v_j \in \Omega\}\ , \quad \partial V_i = \bar{V_i} \setminus V_i\ .$$

Further, we denote by $\boldsymbol{\nu}_i$ the normal unit vector with respect to ∂V_i and by $|V_i|$ the measure of V_i.
Now we integrate the time discretized versions of the equations (3), (4), (5), (47) (11). Lumping terms w without derivatives, i. e.,

$$\int_{V_i} w\ d\Omega = w_i\ |V_i|\ , \quad w_i = w(v_i)\ , \tag{63}$$

and applying the Gauss-theorem

$$\int_{V_i} \nabla \cdot \mathbf{w}\ d\Omega = \int_{\partial V_i} \boldsymbol{\nu}_i \cdot \mathbf{w}\ d\Gamma\ , \tag{64}$$

to divergence terms, we get for $1 \le i \le n_e$

$$-\int_{\partial V_i} \boldsymbol{\nu}_i \cdot (\varepsilon \nabla\varphi)\ d\Gamma + \int_{\partial V_i \cap \Gamma} \alpha_\varphi(\varphi - \varphi_\Gamma)\ d\Gamma\ = [C + p - n]_i\ |V_i|\ , \tag{65}$$

$$n_{\tau i}\ |V_i| - \int_{\partial V_i} \boldsymbol{\nu}_i \cdot \mathbf{j}_n\ d\Gamma + \int_{\partial V_i \cap \Gamma} \alpha_n(n - n_\Gamma)\ d\Gamma\ = -[R]_i\ |V_i|\ , \tag{66}$$

$$p_{\tau i}\ |V_i| + \int_{\partial V_i} \boldsymbol{\nu}_i \cdot \mathbf{j}_p\ d\Gamma + \int_{\partial V_i \cap \Gamma} \alpha_p(p - p_\Gamma)\ d\Gamma\ = -[R]_i\ |V_i|\ , \tag{67}$$

$$[c_h T_\tau]_i |V_i| + \int_{\partial V_i} \boldsymbol{\nu}_i \cdot \mathbf{j}_q\ d\Gamma + \int_{\partial V_i \cap \Gamma} \alpha_T(T - T_\Gamma)\ d\Gamma\ = H_i\ |V_i|, \tag{68}$$

$$\int_{\partial V_i} \boldsymbol{\nu}_i \cdot \nabla \chi \, d\Gamma - \int_{\partial V_i \cap \Gamma} \alpha_\chi (\chi - \chi_\Gamma) \, d\Gamma + [\frac{\omega^2}{c^2} \varepsilon_{opt}(\omega, v_i) - \beta^2] \chi_i \, |V_i| = 0 \, . \quad (69)$$

In (68) the term H_i on the right hand side contains the divergence expression $T\nabla \cdot (\mathbf{j}_n - \mathbf{j}_p)$ which we shift to the left hand side by partial integration. We obtain

$$[c_h T_\tau]_i |V_i| - \int_{\Gamma_i} \nu_i \cdot [\kappa_L \nabla T + T(\mathbf{j}_n - \mathbf{j}_p)] \, d\Gamma +$$

$$\int_{\partial V_i \cap \Gamma} [\alpha_T (T - T_\Gamma) - T\alpha_n (n - n_\Gamma) - T\alpha_p (p - p_\Gamma)] \, d\Gamma = H_{T_i} |V_i|, \quad (70)$$

with

$$H_T = H - \nabla \cdot (T(\mathbf{j}_n - \mathbf{j}_p)) \, . \quad (71)$$

and where H is defined by (48).

In order to transform the system (65), (66), (67), (70), (69) into a time and space discretized form, it remains to discretize the currents $\mathbf{j}_n, \mathbf{j}_p, \mathbf{j}_q$ and the gradient operator. We can restrict us to demonstrate our approach for $\mathbf{j}_n$ with $\sigma_{np} = 0$.

We consider three cases:

(i) We start with the case of Boltzmann statistics and homogeneous temperature $T = T_0$. Then the state, resp. current equation for electrons can be rewritten as

$$n = N_0 \exp \frac{\varphi + \psi_0 - f_n}{T_0}; \quad \mathbf{j}_n = T_0 \mu_n N_0 \left[\nabla \frac{n}{N_0} - \frac{n}{N_0} \nabla \frac{\varphi + \psi_0}{T_0} \right] \, , \quad (72)$$

where

$$N_0 = \sqrt{N_c N_v} \exp \frac{e_v - e_c}{2T_0} \, , \quad \psi_0 = \frac{\log \frac{N_c}{N_v} - e_c - e_v}{2} \, .$$

For this situation the well-tried discretization schema due to Scharfetter-Gummel [12]

$$\int_{\partial V_i} \boldsymbol{\nu}_i \cdot \mathbf{j}_n \, d\Gamma =$$

$$\sum_{l \, : v_i \in E_l} \left[a_j (\frac{n_j}{N_{0_j}} B(s_j) - \frac{n_i}{N_{0_i}} B(-s_j)) + a_k (\frac{n_k}{N_{0_k}} B(s_k) - \frac{n_i}{N_{0_i}} B(-s_k)) \right]$$

can be used. Here $B(s) = \frac{s}{e^s + 1}$ is the Bernoulli-function, (v_i, v_j, v_k) are the vertices of the element E_l and the quantities

$$a_i = \frac{1}{4|E_l|} (|v_i - v_j|^2 + |v_i - v_k|^2 - |v_j - v_k|^2) \, , \, s_i = \frac{(\varphi + \psi_0)_k - (\varphi + \psi_0)_j}{T_0} \, ,$$

are to be cyclically exchanged.

(ii) Next we consider the case of Fermi-Dirac statistics and again homogeneous temperature T_0. In order to reduce (ii) to (i) we replace N_0, ψ_0 in (72) by

$$N = N_0 \sqrt{\gamma_n \gamma_p}\ , \quad \psi = \psi_0 + 0.5 \log \frac{\gamma_n}{\gamma_p}\ ,$$

where

$$\gamma_n = \frac{\mathcal{F}_{1/2}(\frac{c_n}{T_0})}{\exp \frac{c_n}{T_0}}\ , \quad c_n = \varphi - f_n - e_c\ , \quad \gamma_p = \frac{\mathcal{F}_{1/2}(\frac{c_p}{T_0})}{\exp \frac{c_p}{T_0}}\ , \quad c_p = e_v + f_p - \varphi\ .$$

The correction factors γ_n and γ_p from Boltzmann to Fermi-Dirac statistics have to be updated during the iteration procedure which is needed for solving the nonlinear Euler-backwards system.

(iii) Finally, we consider the most involved case of Fermi-Dirac statistics and non-homogeneous temperature T. We define now

$$\begin{aligned} N &= N_0 \sqrt{\gamma_n \gamma_p \exp\left[\ (e_v - e_c)(1/T_0 - 1)\right]}\ , \\ \psi &= \psi_0 + 0.5[\log \frac{\gamma_n}{\gamma_p} + (e_c + e_v)(1 - 1/T_0)], \end{aligned} \tag{73}$$

where

$$T_0 = \min_{1 \le i \le n_v} T_i,$$

$$\gamma_n = \frac{\mathcal{F}_{1/2}(\frac{c_n}{T})}{\exp \frac{c_n}{T_0}}\ , \quad c_n = \varphi - f_n - e_c\ ,$$

$$\gamma_p = \frac{\mathcal{F}_{1/2}(\frac{c_p}{T})}{\exp \frac{c_p}{T_0}}\ , \quad c_p = e_v + f_p - \varphi\ .$$

Replacing $N_0,\ \psi_0$ in (72) by N, ψ from (73) we can proceed as in (i). However, as in (ii), the correction factors γ_n and γ_p have to be updated iteratively.

6 Solution of the Discretized Equations

6.1 Decoupling, Linearization

The equations (65), (66), (67), (70), (69) form in view of the current discretization approach, described in the last subsection, a coupled system of nonlinear algebraic equations. We solve this system time step by time step and start with initial values

$$\varphi(0, v_i),\ n(0, v_i),\ p(0, v_i),\ T(0, v_i)\ , \chi(0, v_i), \quad i = 1, n_v\ ,$$

such that the discrete Poisson-Equation (65) and the wave-guide equation (69) are satisfied. To calculate a first iterate of

$$\varphi(\tau, v_i),\ n(\tau, v_i),\ p(\tau, v_i),\ T(\tau, v_i)\ , \chi(0, v_i), \quad i = 1, n_v\ , \quad \tau > 0\ ,$$

we start solving the continuity equations (66) and (67) to update the quasi-Fermi potentials f_n and f_p. Next we calculate the potential φ by using the

discretized, with respect to φ linearized current conservation equation. We repeat this iteration up to the numerical defects of the equations are sufficiently small. Then we solve (69) and (70) and pass over to the next time step. By 'freezing' the material coefficients depending on the solution at the foregoing time step, we solve during that iteration process only decoupled linear algebraic equations.

6.2 Solution of Linear Algebraic Equations

For solving the decoupled linear algebraic equations we apply sparse matrix techniques. Hereby new factorizations are made so rare as possibly.

7 Example

In the modeling of semiconductor lasers combinations of several effects need to be considered to explain experimental results [13], [14]. Moreover, experimental findings have to be used for the calibration of simulation parameters, which are often not well known. To decrease the number of uncertain simulation parameters, we have simulated separately properties of the strained MQW active region by eight-band kp calculations [4]. In particular, we have computed the optical response function as well as other properties of the strained MQW active region of III-V semiconductor lasers by kp calculations with WIAS-QW [15]. Results from these calculations entered the device simulations with WIAS-TeSCA in terms of net coefficients which allowed to to treat the quantum wells like classical materials with specific material parameters [4].

We consider a structure similar to that described in [16]. It is a long-wavelength InP-based (substrate) ridge waveguide semiconductor laser. The active region is a $Ga_xIn_{1-x}As_yP_{1-y}$ strained MQW structure which is designed for emission at 1.55μm. The structure consists of six 1% compressively strained 7 nm thick quantum wells ($x = 0.239, y = 0.826$), which are separated by 10 nm thick 0.3% tensile strained barriers ($x = 0.291, y = 0.539$).

The active region is sandwiched between two undoped $Ga_xIn_{1-x}As_yP_{1-y}$ ($x = 0.1732, y = 0.3781$) waveguide layers. The lower waveguide layer (n-side) has a thickness of 250nm, whereas the upper waveguide layer (p-side) has a thickness of 180nm.

A part of the transverse cross section is shown in Fig. 3. Let us note that there the lateral coordinate x and the vertical coordinate y are not equally scaled. The quantum well structure (6 Quantum Wells embedded between 7 barriers) is centered in $y = 0$ (dark gray), the upper and lower wave guide layers are highlighted (some lighter gray).

The ridge has a width of 2.4 μm and is highly p-doped ($> 10^{18}/cm^3$), where the p-doping increases up to $> 10^{20}/cm^3$ close to the p-contact. The layers below the lower waveguide are n-doped with nominally $10^{18}/cm^3$.

At the contacts we allowed for a heat-flow (see Fig.3), no thermal isolation of the device has been assumed. The thermal resistance of the top contact is

low. Besides the top of the ridge the p-contact has been passivated by a 200nm SiN_x layer which is also shown in Fig. 3.

The length L of the device was 400μm, a longitudinal scattering loss $\alpha = 10/\text{cm}$ has been assumed as well as reflectivities of $R_0 = R_L = 0.3$ at the end facets of the laser.

7.1 Stationary Characteristics

Throughout all the calculations for this structure single mode emission has been observed. The second transverse mode shown in Fig.3 has been calculated for control but it never came to the threshold. Therefore it's power could be neglected compared to that of the lasing mode.

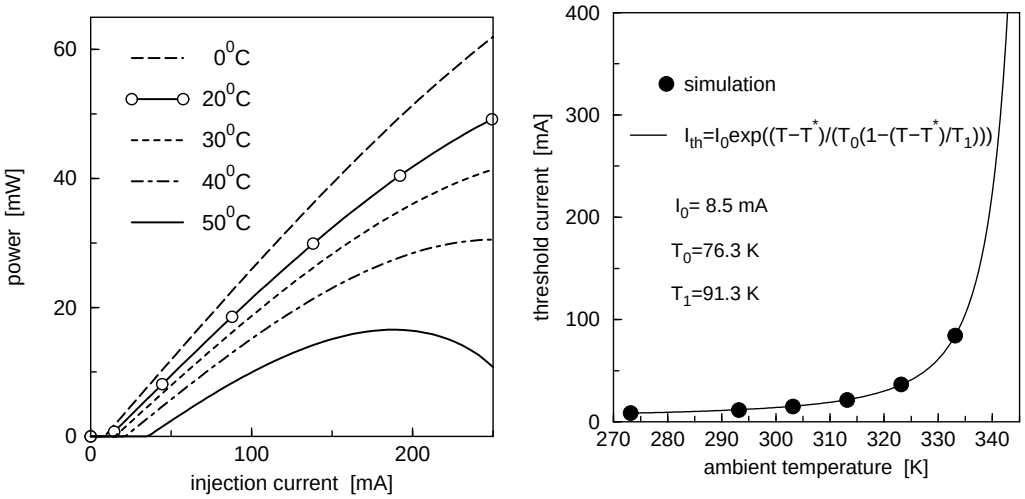

Fig. 1. *Left: PI-characteristics of the device for different ambient temperatures. Above* 50 °C *a significant thermal roll-over occurs. Right: Dependence of the threshold current on the ambient temperature for the above device. Points: Calculation with* `WIAS-TeSCA`*, line: fit according to the modified* T_0*–rule* (74).

Fig.1 displays the calculated P-I characteristics of the device. The influence of self-heating can be detected by the curvature of the P-I curves, which becomes significant in the region above 100mA. The ambient temperature influences the device characteristics too, it's impact is indicated by the different lines in Fig.1 where a significant thermal roll-over for high ambient temperatures occurs. The threshold current grows roughly exponentially with the ambient temperature T, for which we have found a fit by

$$I_{th}(T) = I_0 \cdot \exp\left((T - T^*)/(T_0(1 - (T - T^*)/T_1))\right) \tag{74}$$

with I_0 =8.5mA, T_0 =76.3K, T_1 =91.3K and T^* =273.15K which is displayed in Fig.1 right. This fit very precisely reproduces the simulation results, whereas a fit to the usual exponential T_0-law had been much worse. The latter coincides with (74) at $T = T^*$ to yield a T_0 =76.3K at 0°C, but this usual T_0 would decrease with rising temperature, according to (74). The formula (74) correctly

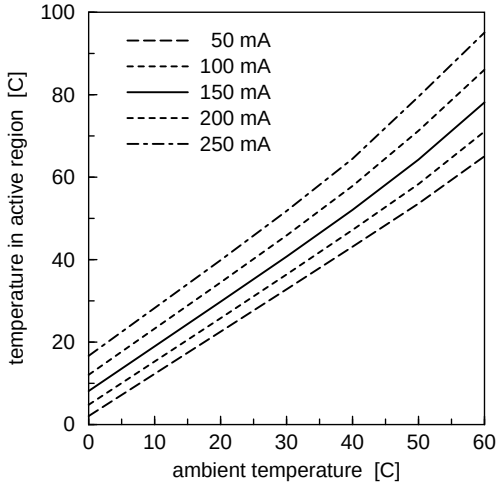

Fig. 2. *Maximum temperature (in the active region) vs. ambient temperature for different injection currents.*

displays that the threshold becomes infinite large at $T = T_1 + T^*$. In practice there is no lasing threshold above 345 K in our example.

Throughout all calculations above threshold, at least in the thermal regime, the maximum temperature was located in the active region close to the peak position of the lasing mode (c.f. Fig.3). The evolution of this maximum temperature (in the active region) with the ambient temperature is displayed in Fig.2 for different injection currents. A super-linear increase can be observed there. Once the temperature rises the optical gain would decrease, but it is in fact not allowed for, due to the realization of lasing threshold. The required compensation can only be realized by a higher carrier density in the active region. The higher carrier density in turn increases the recombination processes (especially Auger) and hence the recombination heating. Moreover, the recombination coefficients and the background absorption itself depend on the temperature (see Appendix). Altogether, this causes the super-linear increase of the maximum temperature with the ambient temperature as well as with the injection current as displayed in Fig.2.

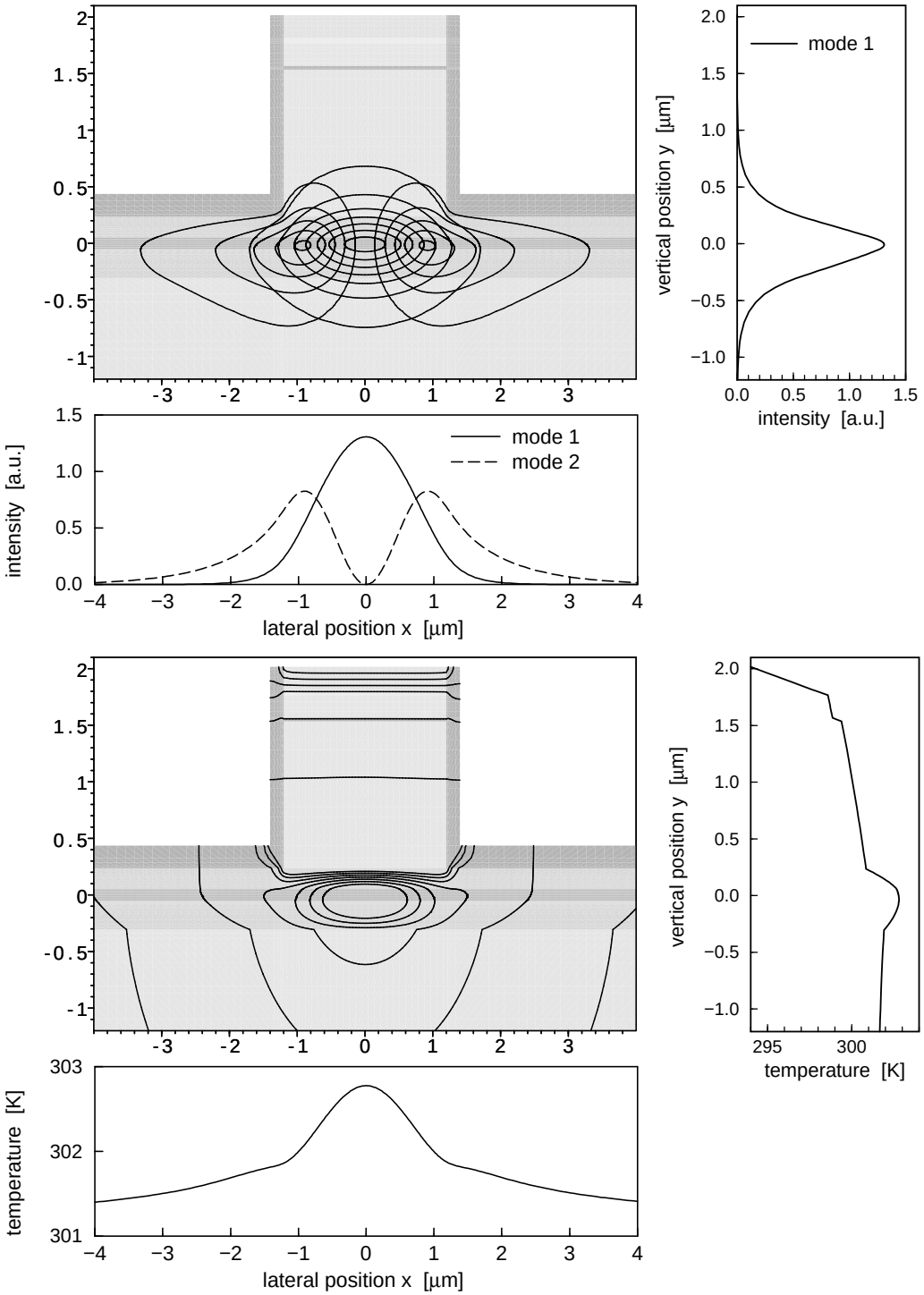

Fig. 3. *Simulation results for given injection current* 150 mA *and ambient temperature* 293 K. *We show isolines in a part of the cross section, the lateral distribution for* $y = 0$ *(in the middle of the QW structure) and the vertical distribution for* $x = 0$ *(in the middle of the ridge) for the intensity pattern of the first and second optical mode (top) as well as for the device temperature (bottom).*

7.2 Modulation Response

Finally let us note that `WIAS-TeSCA` allows to study the small-signal modulation response of the device by performing the AC analysis (linearization of all equations in some fixed operating point characterized by the injection current and the ambient temperature, transformation into the frequency domain). The result of such a simulation is the complex normalized frequency response function $H_n(f)$ where f denotes the frequency of the small modulation of the injection current. Some results are given in Fig. 4 for some fixed ambient temperature and some fixed injection current, respectively.

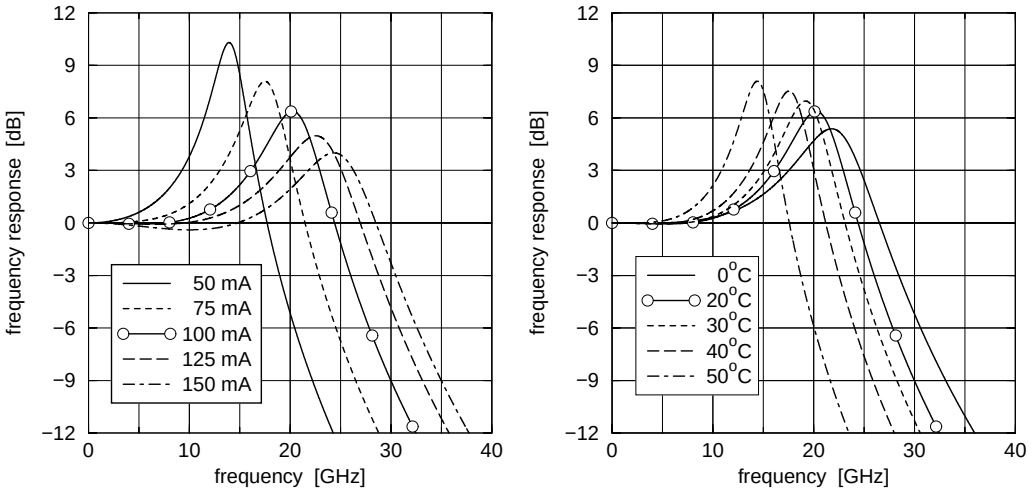

Fig. 4. *Frequency response functions* $10\lg|H_n(f)|^2$ *for given ambient temperature* $20\,^\circ\mathrm{C}$ *and different injection currents (left) as well as for given injection current* $100\,\mathrm{mA}$ *and different ambient temperatures (right).*

We found out, that the function $H_n(f)$ can be very well fitted by the expression

$$H_n(f) = \frac{1}{1+\mathrm{j}\tau_1 f}\,\frac{1}{1+\mathrm{j}\tau_2 f}\,\frac{f_r^2}{f_r^2 - f^2 + \mathrm{j}\gamma_r f} \tag{75}$$

where the parameters τ_1, τ_2, f_r, γ_r depend on the injection current and on the ambient temperature. The last factor in (75) is well known from rate equation models while the other factors are low pass filters due to parasitic effects. The order of magnitude of τ_1 and τ_2 is about 10 ns and 60 ns, respectively. In Fig. 5 there are shown the values of f_r and γ_r which correspond to the curves drawn in Fig. 4.

In the figure on the left f_r^2 and γ_r are linear functions of the injection current I for $< 125mA$ as one would expect for the "non-thermal" regime. Above 125mA heating effects come into play and yield a sub-linear dependence of f_r^2 and γ_r on I. In the right figure especially the dependence of f_r on the ambient temperature is rather complicated and can not simply be expressed by a power law.

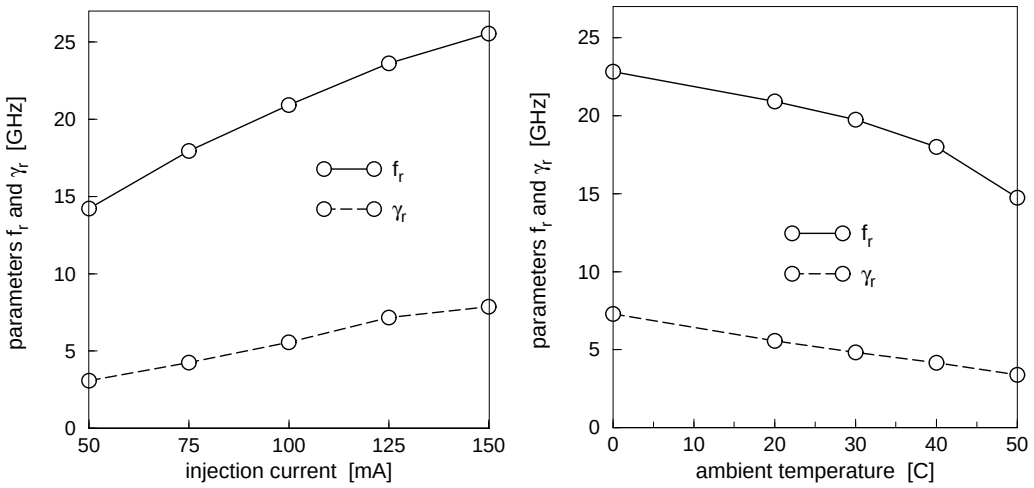

Fig. 5. *Extracted parameters f_r and γ_r for given ambient temperature* 20 °C *and different injection currents (left) as well as for given injection current* 100 mA *and different ambient temperatures (right).*

8 Conclusion

We have derived a thermodynamics-based model for edge-emitting quantum well lasers. The model comprises the drift-diffusion equations, the Poisson equation as well as equations for the optical field, which have been discussed in detail. Following basic thermodynamic principles we have accomplished this model by the heat flow equation (47). In deriving this equation we started with an energy balance equation and general expressions for the densities of the energy and the entropy. Following Lagangre's method and the maximum entropy principle we first defined the thermodynamic equilibrium. Then, by applying the principle of local thermal equilibrium and taking into account the second law of thermodynamics as well as the Onsager symmetry relations we obtained expressions for the current densities which guided us at least to the desired heat flow equation (47). Boundary conditions as well as proper discretization schemes have been given explicitly and discussed with respect to the solution procedure. The self-consistent numerical solution of the full problem can be obained by our code WIAS-TeSCA, which is a software for the numerical simulation of semiconductor devices. Using WIAS-TeSCA, we have demonstrated the simulation of a long-wavelength ridge-waveguide multi-quantum well laser, with a special focus on the self-heating of the device and its modulation response.

Appendix Temperature Dependence of Model Parameters

Spontaneous radiative recombination:

$$R^{sp} = B \cdot (n \cdot p - n_i^2) \tag{76}$$

$$B(T) = B_0(T/T_0) \tag{77}$$

$B_0 = 4 \cdot 10^{-10}/\mathrm{cm}^3\mathrm{s}$, $T_0 = 300\mathrm{K}$.
Auger Recombination:

$$R^{AUG} = (C_n n + C_p p) \cdot (n \cdot p - n_i^2) \tag{78}$$

$$C(T) = C_0 \left(\frac{kT}{E_a}\right)^{\gamma} \exp\left(\frac{E_a}{kT_0} - \frac{E_a}{kT}\right) \tag{79}$$

$C_0 = 4 \cdot 10^{-28}/\mathrm{cm}^6\mathrm{s}$, $E_a = 0.5\mathrm{eV}$, $T_0 = 300\mathrm{K}$.
Background Absorption $\alpha_{bg} = \alpha_{IVB} + f_{cn} \cdot n + f_{cp} \cdot p$.
Intervalence Band Absorption:

$$\alpha_{IVB}(T) = \alpha_0 \exp\left(\frac{E_a}{kT_0} - \frac{E_a}{kT}\right) \tag{80}$$

$\alpha_0 = 80/\mathrm{cm}$ (in quantum wells), $E_a = 0.1\mathrm{eV}$, $T_0 = 300\mathrm{K}$.
Free Carrier Absorption: $f_{cn} = f_{cp} = 10^{18}\mathrm{cm}^2$.
Refractive Index:

$$n(T) = n_0 + n' \cdot \left(\frac{T - T_0}{kT_0}\right), \tag{81}$$

$n' = 6.8 \cdot 10^{-4}$, $T_0 = 300\mathrm{K}$. For the above calculations we have used a very simple gain model that approximates the gain in the vicinity of its spectral maximum under the constraint $E_g \approx \hbar\omega$:

$$g = \kappa \cdot \left[\exp\left(\frac{f_p - f_n - \hbar\omega}{kT}\right) - 1\right] \cdot \frac{np}{n_i^2} \exp\left(\frac{f_n - f_p}{kT}\right) \tag{82}$$

The factor

$$\frac{np}{n_i^2} \exp\left(\frac{f_n - f_p}{kT}\right)$$

is $= 1$ in the Boltzmann case and ≈ 1 in the Fermi case. Therefore the prefactor determines the gain maximum and has been adjusted to $\kappa = 3000/\mathrm{cm}$ throughout our calculations.

References

1. G. K. Wachutka. Rigorous treatment of heat generation and conduction in semiconductor device modeling. *IEEE Transactions CAD*, 9:1141, 1990.
2. G. Albinus, H. Gajewski, and R. Hünlich. Thermodynamic design of energy models of semiconductor devices. *Nonlinearity*, 15:367–383, 2002.
3. WIAS-TeSCA. http://www.wias-berlin.de/software/tesca, 2003.
4. U. Bandelow, R. Hünlich, and T. Koprucki. Simulation of Static and Dynamic Properties of Edge-Emitting Multi Quantum Well Lasers. *IEEE Journal of Selected Topics in Quantum Electronics*, 9(3):798–806, May/June 2003.
5. H. J. Wünsche, U. Bandelow, and H. Wenzel. Calculation of combined lateral and longitudinal spatial hole burning in $\lambda/4$ shifted DFB lasers. *IEEE Journal of Quantum Electronics*, 29(6):1751–1761, 1993.
6. L. D. Landau and E. M. Lifschitz. *Course of Theoretical Physics*, volume V: "Statistical Physics". Pergamon Press, London, 3 edition, 1971–.
7. S. L. Chuang. *Physics of optoelectronic Devices*. Wiley & Sons, New York, 1995.
8. C. H. Henry and R. F. Kazarinov. Quantum noise in photonics. *Reviews of Modern Physics*, 68(3):801–853, 1996.
9. T. T. Mnatsakanov. Transport Coefficients and Einstein Relation in a High Density Plasma of Solids. *physica status solidi (b)*, 143:225, 1987.
10. D. E. Kane and R. M. Swanson. Modeling of Electron–Hole Scattering in Semiconductor devices. *IEEE Transactions on Electron Devices*, 40:1496, 1993.
11. J. Piprek. *Semiconductor Optoelectronic Devices: Introduction to Physics and Simulation*. Academic Press, 2003.
12. D. L. Scharfetter and H. K. Gummel. Large–Signal Analysis of a Silicon Read Diode Oscillator. *IEEE Transactions on Electron Devices*, 16:64, 1969.
13. M. Grupen and K. Hess. Simulation of carrier transport and nonlinearities in quantum–well laser diodes. *IEEE Journal of Quantum Electronics*, 34(1):120–140, January 1998.
14. J. Piprek, P. Abraham, and J. E. Bowers. Self-Consistent Analysis of High-Temperature Effects on Strained-Layer Multi-Quantum Well InGaAsP/InP Lasers. *IEEE Journal of Quantum Electronics*, 36(6):366–374, 2000.
15. WIAS-QW. http://www.wias-berlin.de/software/qw, 2003.
16. M. Möhrle, A. Sigmund, J. Kreissl, F. Reier, R. Steingrüber, W. Rehbein, and H. Röhle. Integratable high-power small-linewidth $\lambda/4$ phase-shifted 1.55 μm InGaAsP-InP-Ridge-Waveguide DFB Lasers. In *Workbook of 26th Int. Conf. on Compound Semiconductors (ISCS'99), Berlin, Germany*, page Th A3.1, 1999.